Journal of CO_2 Utilization 24 (2018) 81–88

Contents lists available at ScienceDirect

Journal of CO_2 Utilization

journal homepage: www.elsevier.com/locate/jcou

Photoelectrocatalytic performance of nanostructured p-n junction $NtTiO_2$/NsCuO electrode in the selective conversion of CO_2 to methanol at low bias potentials

Juliana Ferreira de Brito*, Felipe Fantinato Hudari, Maria Valnice Boldrin Zanoni

São Paulo State University (UNESP), Institute of Chemistry, R. Francisco Degni 55, 14800-060, Araraquara, SP, Brazil

ARTICLE INFO

Keywords:
CO_2 reduction
Nanostructured $NtTiO_2$/NsCuO semiconductor
Methanol formation
p-n junction
Photoelectrocatalysis mechanism

ABSTRACT

Aiming a selective reduction of CO_2 to methanol, a p-n junction semiconductor was constructed based on CuO nanospheres (NsCuO) deposited at TiO_2 nanotubes ($NtTiO_2$). The $NtTiO_2$/NsCuO material demonstrated smaller charge transfer resistance, smaller flat band potential and wider optical absorption when compared with $NtTiO_2$ and/or Ti/TiO_2 nanoparticles coated by higher size particles of CuO (Ti/TiO_2/CuO). The selective reduction of dissolved CO_2 to methanol was promoted at lower potential of +0.2 V and UV–vis irradiation in 0.1 mol L^{-1} K_2SO_4 electrolyte pH 8 with 57% of faradaic efficiency. Even though the performance of the nanostructured material $NtTiO_2$/NsCuO was similar to the non-completely nanostructured material Ti/TiO_2/CuO (0.1 mmol L^{-1} methanol), the conversion to methanol has been significantly increased when hydroxyls (0.62 mmol L^{-1}) and holes scavengers (0.71 mmol L^{-1}), such as p-nitrosodimethylaniline (RNO) or glucose, respectively, were added in the supporting electrolyte. It indicates that photogenerated electron/hole pairs are spatially separated on p-n junction electrodes, which produces effective electrons and long-life holes, influencing the products formed in the reaction. A schematic representation of the heterojunction effect on the photoelectrocatalytic CO_2 reduction is proposed under the semiconductor and each supporting electrolyte, which improves the knowledge about the subject.

1. Introduction

The pursuit for solution to global warming and use of fossil fuel has demanded great interest in the conversion of CO_2 to fuels [1–4]. The recent advances in the understanding of the role of photoelectrocatalytic devices, semiconductors and photoelectrocatalytic processes in the development of solar fuels from water and CO_2 is reviewed in the literature [5–9]. However, the great challenge is to design systems able to promote the capture of solar radiation and conversion of CO_2 into fuels that can be easily stored. On this basis, photoelectrocatalysis for CO_2 reduction has gained significant attention in the last five years due to its high efficiency and the high-value products generated [1–4,10], but it still offers lack of efficiency and low selective reactions to just one high-value product [11].

The photoelectrocatalytic conversion of dissolved CO_2 in aqueous solution is complex. A high efficiency can be obtained for catalyst with high ability to chemisorb and activate the CO_2 and it depends of (i) the semiconductor type used as photocathode [[3],12,13], (ii) the irregularities of the surface that can display different CO_2 adsorption modes [14], (iii) the supporting electrolyte [3], (iii) the pH of the solution [12], (iv) the applied potential [13], (v) the photoelectrocatalysis time [15], the photoelectrocatalytic reactor design [[3],15,17,18] and others.

Thermodynamically, the reduction of CO_2 takes place faster under semiconductor that presents conduction band edge more negative than the redox potential for CO_2 reduction and valence band edge lower than redox potential for water oxidation [11,16,17]. Nevertheless, p-type semiconductor commonly demands large potential, once their valence band potentials are not positive enough to oxidize water [18].

Semiconductors based on copper and copper oxides [1,[23],19] are good candidates for that and have shown great success for photoelectrocatalytic reduction of CO_2 to alcohols [[23],16,20,21]. Copper oxides have the ability to act simply as electron traps [22] and present good platform for CO_2 adsorption [23]. Cu^{2+} ion has an unfilled 3d shell, making its reduction thermodynamically feasible. On the other hand, CuO absorbs light in the visible region [24,25], presents specific reductive characteristics [25,26] and can easily trap the electron generated on the other semiconductor surface [13,22]. But, they can show low stability under reductive conditions and light [27].

The photoelectrocatalytic reduction of carbon dioxide is a multiple

* Corresponding author.
E-mail address: jfbrito@ymail.com (J.F.d. Brito).

https://doi.org/10.1016/j.jcou.2017.12.008
Received 28 July 2017; Received in revised form 2 November 2017; Accepted 9 December 2017
Available online 16 December 2017

step process, limited for the adsorption of CO_2 on the electrode surface. The steps are based on the transfer of multiple photogenerated electrons (conversion to methanol requires six electrons) and also the formation of hydrogen radical relevant to produce hydrocarbon from carbon dioxide [28]. The literature has reported that p-n junction semiconductors can be a good alternative to enhance the photoelectrocatalytic performance [15,13,29–32]. The heterojunction can enhance the separation of electron-hole pairs, since the charge transfer can be amplified by the Z-scheme mechanism [17,32], facilitating these multiple steps.

The arrangements of copper, copper oxides and TiO_2 have been investigated as effective way to improve the photoreduction of CO_2. A narrow band gaps (E_{bg}) and sufficient Fermi levels (E_f) are capable to reduce CO_2 to CH_3OH ($E_0 \sim -0.4$ V *vs* NHE) in the CuO semiconductor ($E_{CB} \sim -1.75\sim$ and $E_{VB} \sim 0.25$ V *vs* NHE) [13]. The photoactivated electron in the TiO_2 conduction band (CB) ($E_{CB} \sim -0.25$ V and $E_{VB} \sim 3.0$ *vs* NHE) is not able to reduce CO_2–CH_3OH. Because of that, the coupling of two semiconductors (p and n-type) can minimize the recombination due the interaction with the electrons generated in the TiO_2 and holes generated in the valence band (VB) of CuO, a typically z-scheme mechanism [13,17,32]. In addition, holes generated in the VB of TiO_2 perform the water oxidation to H·, which is important to conversion of CO_2 into hydrocarbons and fuels. This TiO_2 and CuO union can increase the shift of light absorption to the visible light region ($E_{bgCuO} \sim 1.7$ eV and $E_{bgTiO2} \sim 3.2$ eV) [13,33] and improve the stability of the CuO catalyst [13,20,34].

Another effect that has presented photoelectrocatalytic upgrade is the use of nanostructured materials [31,17,35]. Among the several possibilities of nanostructures, nanotubes are shown to be the most promisor semiconductor type due to the large surface area and their good electronic transport of the photogenerated electron/hole pairs, reducing the recombination and increasing the efficiency in the process [36,37]. The literature also reports that nanoparticulated films deposited on semiconductor surface can improve the kinetic of holes reaction with electrolyte (due to higher penetration of electrolyte), change the material conductivity and also change the adsorption of analyte on the substrate [38,39].

The aim of the present work is to compare the effect of CuO nanospheres deposited at nanotubes TiO_2 electrode prepared by anodization with a non-nanostructured material, to improve photoelectrocatalytic performance in the selective conversion of CO_2 to methanol at low bias potentials (+0.20 V *vs.* Ag/AgCl for instance) and to understand the mechanism involved in the system. The heterojunction involving catalyst nanoparticle changed charge transfer resistance and separation efficiency at the contact interface semiconductor electrolyte when compared to composites of Ti/TiO_2/CuO without a complete nanostructure. These effects are supported by EIS, photocurrent voltage and also by the improvement of methanol formation analyzed by chromatographic techniques.

2. Experimental

2.1. Preparation of CuO nanospheres-decorated TiO_2 nanotubes electrode ($NtTiO_2$/NsCuO)

TiO_2 nanotube arrays electrode was prepared by electrochemical anodization in aqueous solution [40]. A titanium plate with 4.0 cm^2 was polished using abrasive papers of successively finer roughness and then cleaned by applying three 15 min steps in sonication with acetone, isopropanol and ultrapure water. The cleaned plate was dried in a N_2 stream. Electrochemical anodization was performed in a two-electrode cell using a ruthenium foil as the counter electrode and 1.0 mol L^{-1} NaH_2PO_4 + 0.3 wt.% HF as the supporting electrolyte. The applied potential was initially ramped from 0 to 20 V at 2 V min^{-1} and then kept constant at 20 V for 2 h. After the anodization, the electrode was cleaned with ultrapure water, dried with a N_2 stream and annealed at 450 °C for 2 h.

After annealing, the TiO_2 nanotubes were decorated with CuO nanospheres by dip coating using an adapted methodology [41]. The decorated semiconductor was obtained following two depositions of copper oxide by dip coating. The solution used for the dip coating was prepared with dibasic copper carbonate (8.4×10^{-2} mol L^{-1} of metal) as a copper oxide precursor, citric acid and ethylene glycol in a metal molar ratio of 1:4:16, respectively. The semiconductor was annealed after each deposition at 450 °C for 2 h.

The Ti/TiO_2/CuO semiconductor without nanostructure was obtained by dip coating of six layer with copper oxide and titanium oxide precursors following by annealing after each deposition [13,41]. This material results of characterization and CO_2 reduction under different potential and supporting electrolytes was publish recently by the authors [13]. The Ti/TiO_2/CuO electrode presents 10% in weight of CuO semiconductor [13], three times higher than is coating in the $NtTiO_2$/NsCuO.

2.2. Characterization of ($NtTiO_2$/NsCuO)

The prepared semiconductor was characterized structurally and morphologically by X-ray diffraction (XRD) on a Siemens D5000 diffractometer with Cu Kα radiation and Field Emission Gun-Scanning Electron Microscopes (FEG-SEM) on a JEOL 7500F Microscope coupled to energy-dispersive X-ray spectroscopy analysis (EDS). An UV/Vis/NIR spectrometer (PerkinElmer Lambda 1050) with an Integrating Sphere-150 mm UV/Vis/NIR (InGaAs) module for diffuse reflectance measurements was used to obtain the optical band gap.

The electronic charge transfer was analyzed by electrochemical impedance spectroscopy (EIS) in an Autolab PGSTAT 302N potentiostat with Nova 1.11.2 software (Metrohm Autolab B.V.). The measurements were performed using a Ag/AgCl reference electrode and a Pt counter electrode in 5.0 mmol L^{-1} $Fe(CN)_6^{3-/4-}$ prepared in 0.1 mol L^{-1} KCl as supporting electrolyte. The frequency employed range from 10 kHz to 0.03 Hz, with a 5 mV rms sinusoidal modulation at 0.22 V.

The photocurrent response was evaluated by linear sweep voltammetry in 0.1 mol L^{-1} $NaHCO_3$ at pH 8 with and without CO_2 using at scan rate of 0.01 V s^{-1} using an Autolab PGSTAT 302.

2.3. CO_2 Reduction by photoelectrocatalysis

The photoelectrocatalytic reduction of CO_2 was performed in a two compartments reactor of 200 mL in each compartment (Fig. 1), separated by a nafion® proton exchange membrane (6). An electrode of $NtTiO_2$/NsCuO acting as photocathode (working electrode) (1) was positioned in a compartment receiving the incidence of light system (UV–vis light from a commercial 125 W high pressure mercury lamp without the bulb with I = 9.23 W m^{-2}) through a quartz window (7). An Ag/AgCl reference electrode (2) was also inserted in the same compartment where, CO_2 was also bubbled (1.0 mL min^{-1}) (3) continuously during 45 min to reach saturation and maintained during all the experiment. A Pt grid was used as a counter electrode (4) and the

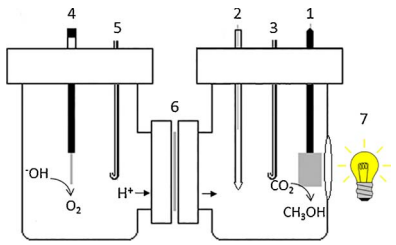

Fig. 1. Scheme of the two compartments photoelectrocatalytic reactor used for CO_2 reduction. 1) photocathode, 2) reference electrode (Ag/AgCl), 3) CO_2 bubbling, 4) counter electrode (Pt grid), 5) gas bubbling, 6) nafion® proton exchange membrane and, 7) UV–vis light incidence by a quartz window.

solution of the counter electrode compartment cell was also the same that in the working compartment, but it was deaerated with N_2 (5). The CO_2 reduction was performed under 0.1 mol L^{-1} K_2SO_4 solution pH 8, 0.1 mol L^{-1} K_2SO_4 with 0.05 mmol L^{-1} p-nitrosodimethylaniline (RNO) solution pH 8 and, 0.1 mol L^{-1} K_2SO_4 with 10.0 mmol L^{-1} glucose solution pH 8 as the supporting electrolytes. The photoelectrocatalytic reduction of CO_2 was carried out during 180 min and aliquots of the catholyte and anolyte were removed and analyzed after 15, 30, 60, 120 and 180 min.

2.4. Analysis of CO_2 reduction products

Methanol was analyzed by gas chromatography on a Model CG-2010 Schimadzu instrument coupled with a flame ionization detector (CG-FID) employing a solid-phase micro-extraction technique (SPME) [3]. For this purpose, samples of 0.5 mL of the photoelectrolyzed solution was transferred to a sealed container (1.5 mL) and submitted to a heated bath for 7 min at 65 °C. Afterwards, the fiber (75 μm Carboxen/PDMS, SUPELCO) was exposed to the container vapors for 5 min and the fiber was directly injected into the gas chromatograph. The chromatographic column employed was a Stabilwax RESTEC of 30 m length, 0.25 mm internal diameter and 25 mm film thickness. N_2 was used as the carrier gas at a 1.0 mL min^{-1} flow rate. The temperature of the injector was maintained at 250 °C and the detector at 260 °C in splitless mode. The heating ramp used was: 40 °C hitting at 2 °C min^{-1} until 46 °C and 45 °C min^{-1} until 170 °C for 3 min. An analytical curve was constructed with linear relationship from 0.2 μmol L^{-1} to 10 mmol L^{-1} for methanol. The determination coefficients and quantification limits were 0.9723 and 0.2 μmol L^{-1}, respectively.

Ethanol (C_2H_5OH) and acetone (CH_3COCH_3) were analyzed by the same CG-FID methodology. Formic acid (HCOOH) and acetic acid (CH_3COOH) were analyzed by liquid chromatography coupled to a diode-array detector (HPLC) on a Model 10AVP Shimadzu equipped with a Rezex ROA-Organic Acid H^+ (8%) column flowing the 210 nm wavelength. The mobile phase was 2.5 mmol L^{-1} H_2SO_4 at flow rate of 0.5 mL min^{-1} under room temperature. Formaldehyde (HCOH) and acetaldehyde (CH_3COH) were analyzed by HPLC using methodology described in our previous work [12].

The OH production was followed by using 0.05 mmol L^{-1} RNO solution (Sigma-Aldrich, 97%) as bleaching reaction, once RNO is a well-known OH radical trapping [42]. The RNO decay was monitored by UV–vis spectrophotometry analysis (Agilent, Cary 60) at 440 nm.

3. Results and discussion

3.1. Characterization of $NtTiO_2$ decorated by NsCuO

Fig. 2 illustrates the FEG-SEM image of TiO_2 nanotubes ($NtTiO_2$) top view before modification (Fig. 2a) and after decoration with CuO nanospheres (Fig. 2b). Self-organized TiO_2 nanotubes prepared using aqueous methodology are coated on Ti plate with an average diameter of 90 nm, wall thickness of 20 nm and medium length of 900 nm [42,43]. Deposits of CuO nanospheres of average size of 39 nm were well-distributed on the nanotube wall, as shown in Fig. 2b.

XRD and EDS (Fig. 3a and b, respectively) confirm the occurrence of these deposits of CuO. The crystallinity of the obtained material is confirmed by the defined peaks at 2θ = 25.3, 54.2, 70.6 and 92.8° attributed to anatase phase of TiO_2 (A), 2θ = 40.2° and 76.2° attributed by the presence of Ti substrate (T) and 2θ = 35.4 and 82.6° attributed by occurrence of CuO (C), respectively. The EDS analysis (Fig. 3b) confirms the presence of Cu (0.8, 8.0 and 8.8 keV), O (0.4 keV) and Ti (0.3, 4.5 and 4.9 keV), constituents of $NtTiO_2$/NsCuO.

Fig. 4a compares the diffuse reflectance spectra (DRS) recorded for $NtTiO_2$ and $NtTiO_2$/NsCuO electrodes. Deposits of CuO nanospheres promoted a slight decrease in the absorbance at wavelength (λ) lower than 350 nm, but the light absorption increased the absorption intensity at visible light (λ > 420 nm). The results confirm that heterojunction of n-type TiO_2 nanotubes and p-type CuO nanospheres semiconductors can wider the optical absorption of the new material [20,28].

The band gap energy estimated for both electrodes (insert of Fig. 4a) using kubelka-Munk equation [44] indicated that CuO nanosphere (Ebg ~ 1.4 Ev [45,46]) deposited on TiO_2 nanotubes surfaces (Ebg ~ 3.0 Ev [47–49]) shifted the band gap energy to approximately 2.3 eV. This indicates that probably decoration of TiO_2 nanotubes by CuO nanoparticles could introduces new acceptor level in the band gap as intermediate states, making it more efficient as electron trap [22]. In addition, there are loss of transparency in the new material when irradiated by visible light [50–52], which can improve the photoelectrocatalytic response when irradiated by a commercial lamp

The effect of applied potential on photocurrent curves of I_{ph} *vs.* E (Fig. 4b) were recorded at scan rate of 10 mV s^{-1} in 0.1 mol L^{-1} $NaHCO_3$ pH 8 saturated with CO_2 for the $NtTiO_2$/NsCuO electrode in the dark (curve I) and UV–vis irradiation (curve III). For comparison, the same experiment was carried out for Ti/TiO_2/CuO semiconductor, where the TiO_2 are deposited as nanoparticles and CuO has a dimension of 300 nm (curve II) [13]. Under dark, $NtTiO_2$/NsCuO electrode (curve I) presented no current flow at anodic potential and the current flow at potentials more negative than −1.0 V is associated with hydrogen evolution [12]. However, under UV–vis irradiation the curves of I_{ph} *vs.*

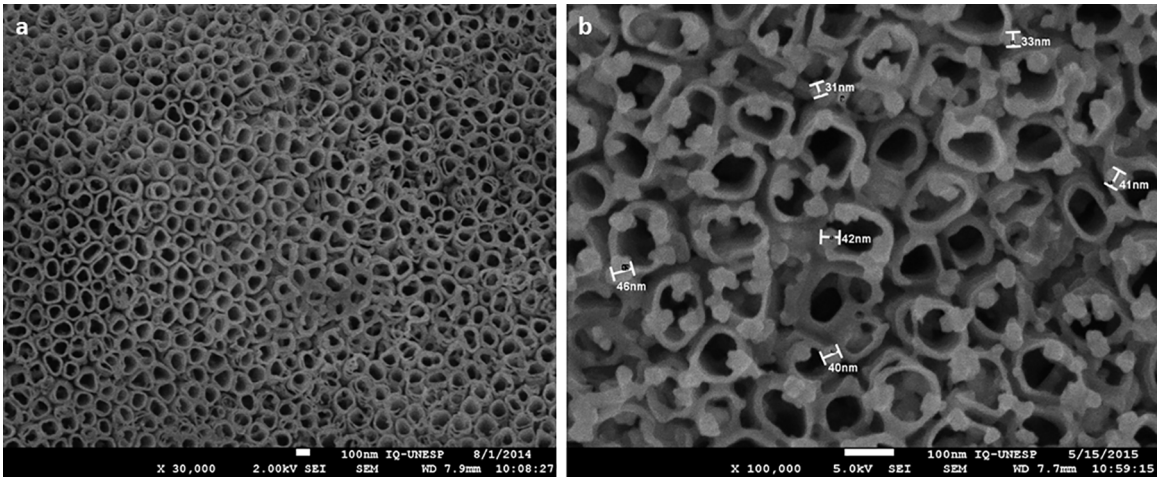

Fig. 2. FEG-SEM image of the top view of (a) TiO_2 nanotubes without modification and (b) TiO_2 nanotubes with copper II oxide nanoparticles.

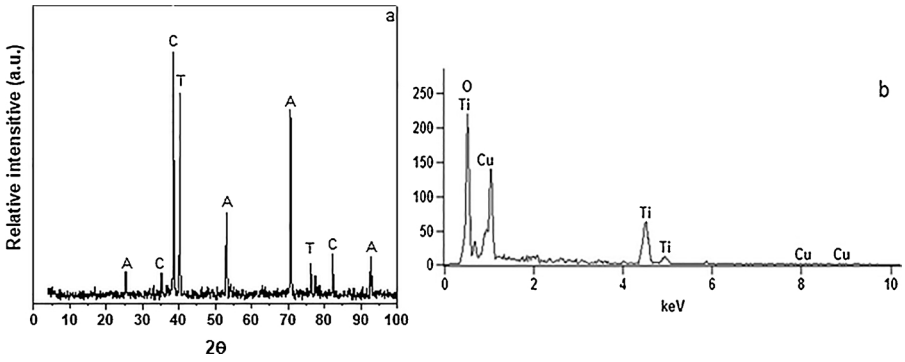

Fig. 3. (a) XRD diffractograms and (b) EDS of the TiO_2 nanotubes decorated with two dip coating layers of CuO nanospheres semiconductor.

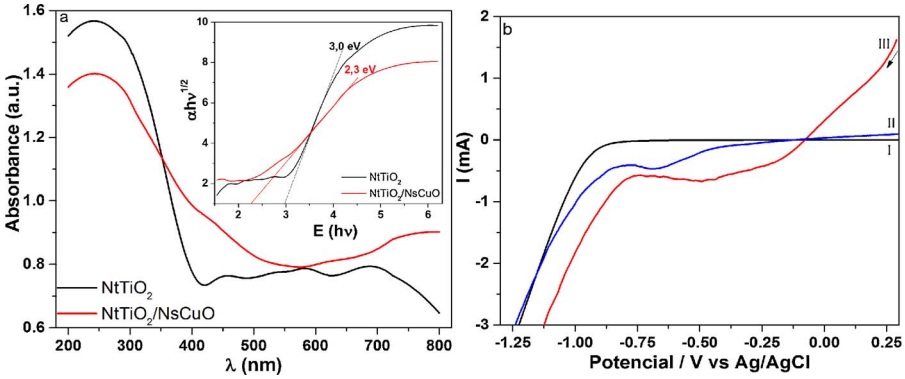

Fig. 4. (a) Diffuse reflectance analysis of TiO_2 nanotubes (black line) and $NtTiO_2$/NsCuO (red line) with the insert of band gap for TiO_2 nanotubes (black line) and $NtTiO_2$/NsCuO (red line); b) photocurrent *vs.* potential of the $NtTiO_2$/NsCuO electrode in the dark (I - black curve) and under UV-Vis light (III - red curve), compared with Ti/TiO_2/CuO electrode under UV-Vis light (II - blue curve), under supporting electrolyte saturated with CO_2 in all of the curves. (For interpretation of the references to colour in this figure legend, the reader is referred to the web version of this article.)

E of $NtTiO_2$/NsCuO electrode (curve III) presented a typical behavior of a p-n junction electrode. A high anodic current density is observed at potential higher than −0.1 V *vs* Ag/AgCl reaching a current of 1.5 mA at +0.2 V [[13],12,13]. This current is about 10 times higher than the Ti/TiO_2/CuO, indicating that the nanotubes and the size of the nanoparticle facilitate the separation of photogenerated charges and interfacial transfer of electron. These behavior is an indicative that could be possible to reduce CO_2 at bias potential so low as +0.2 V *vs* Ag/AgCl. In addition, at negative potential is observed a shift of 200 mV for CO_2 reduction at $NtTiO_2$/NsCuO in relation to Ti/TiO_2/CuO electrode. It is an indicative that electrons are photogenerated on irradiated $NtTiO_2$/NsCuO, that are rapidly trapped by adsorbed CO_2 at CuO nanoparticles [33].

In order to evaluate how the particle size interferes in the interfacial charge transfer resistance (R_{CT}), electrochemical impedance spectroscopy (EIS) measurements (Fig. 5a) were carried out in 5.0×10^{-3} mol L^{-1} $Fe(CN)_6^{3-/4-}$ redox probe (0.1 mol L^{-1} KCl) for the semiconductors $NtTiO_2$/NsCuO (black curve) and Ti/TiO_2/CuO (red curve). For comparison, it was also recorded EIS for $NtTiO_2$ without any modification (blue curve). Fig. 5a shows the Nyquist plots, where the diameter of the semicircle obtained is related to electrons transfers and separation of the electron/hole pairs generated at the electrode interface (semiconductor/electrolyte) [53,54]. The insert in the Fig. 5a compares the reduction in the charge transfer resistance for the nanostructured electrode $NtTiO_2$/NsCuO, for Ti/TiO_2/CuO semiconductor and for $NtTiO_2$ without modification. The semicircle diameter is much smaller for heterojunctions using TiO_2 nanotubes and CuO nanospheres coatings, indicating that the separation of photogenerated charges is facilitated in the Schottky barriers.

The value of R_{CT} estimated for the nanostructured $NtTiO_2$/NsCuO semiconductor was 1.34 KΩ, while for the semiconductor with the same oxides, but non-completely nanostructured (Ti/TiO_2/CuO), the electrical resistance change was 905 KΩ, and for the $NtTiO_2$ without modification was 11.3 MΩ. The value of charge transfer resistance for the heterojunction between copper oxide nanospheres and TiO_2 nanotubes is decreased when compared with $NtTiO_2$ and Ti/TiO_2/CuO, proving that the better performance is obtained for the completely nanostructured material.

To a better understanding of the effect of NsCuO on the performance of composite, potential-dependent capacity measurements were recorded for $NtTiO_2$/NsCuO and $NtTiO_2$ electrodes in 0.1 mol L^{-1} phosphate buffer solution pH 7 at 10 Hz, as shown in Fig. 5b. The flat band potential (U_{fb}) and the carrier's densities (N_D) were calculated using the Mott-Schottky plots by the equation:

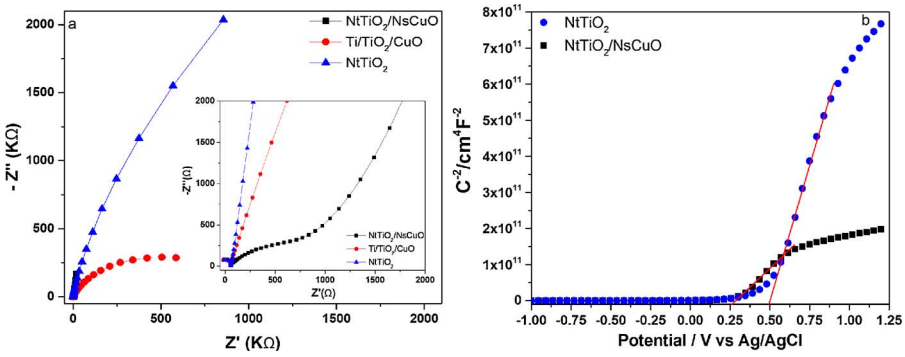

Fig. 5. a) EIS measurements in 5.0×10^{-3} mol L^{-1} $Fe(CN)_6^{3-/4-}$ redox probe (0.1 mol L^{-1} KCl) for the semiconductors $NtTiO_2$/NsCuO (black curve), Ti/TiO_2/CuO (red curve) and $NtTiO_2$ (blue curve). Figure insert: Amplification of Nyquist plot; b) C^{-2} *vs.* E relation at 10 Hz in 0.1 mol L^{-1} phosphate buffer solution pH7 for the semiconductors $NtTiO_2$/NsCuO (black curve) and $NtTiO_2$ (blue curve). (For interpretation of the references to colour in this figure legend, the reader is referred to the web version of this article.)

$$C_{SC}^{-2} = \left(2/\varepsilon\varepsilon_0 e N_D\right)\left(E - E_{fb} - kT/e\right) \quad (1)$$

where C_{SC} is the differential capacitance of the space charge layer; ε is the dieletric constant, in the anatase case the value applied was 48; ε_0 is the permittivity in the vacuum (8.86×10^{-14} F cm^{-1}); e is the elementary electron charge (1.6×10^{-19} C); U is the applied bias potential; K is the Boltzmann constant and T is the temperature [55,56].

The flat band potential (E_{fb}) for both semiconductors were obtained from the intercept on the V axis of C^{-2} *vs.* V plot (generating the relation $E_{fb} = E - kT/e$) (Fig. 5b). The E_{fb} for $NtTiO_2$ was 0.46 V, whereas after insertion of CuO nanosphere there was a decrease of 200 mV. The results indicated that in a heterojunction electrode probably the Z-scheme heterojunctions could be preponderant and the electrons photogenerated under irradiation in the TiO_2 semiconductor can be driven to the CuO resulting in significant synergistic effects able to improve the separation of charge and the performance in relation to the CO_2 reduction.

The number of carrier's density was also calculated using the linear region slope of Mott-Schottky plot ($N_D = 2/\varepsilon.\varepsilon_0.e.slope$) [56]. The N_D obtained by the TiO_2 nanotubes without modification was 2.08×10^{18} while for the $NtTiO_2$/NsCuO the N_D was 7.12×10^{18}. In other words, the number of carrier's density is more than three times higher when the electrode is modified ($NtTiO_2$/NsCuO). Thus, the results indicate that the modification of $NtTiO_2$ with CuO nanospheres reduce the material resistance, improve the surface charge transfer and also the Fermi energy (based on E_{fb}) and, therefore, could be a good candidate to be applied in the CO_2 reduction.

3.2. CO_2 reduction at $NtTiO_2$/NsCuO electrode

Taking into consideration that at a negative potential could occur the reduction of CuO nanospheres to metallic copper [26,57,58], and that E_{fb} of the $NtTiO_2$/NsCuO is 0.26 V, further photoelectrocatalytic experiments to promote reduction of CO_2 were carried out in 0.1 mol L^{-1} K_2SO_4 solution pH 8 saturated by CO_2 gas, applying a potential of +0.2 V and UV–vis irradiation. Fig. 6a compares the amount of methanol formed during the time under $NtTiO_2$ electrode and $NtTiO_2$ modified with CuO nanospheres. Fig. 5b shows the methanol concentration formed after 180 min of photoelectrocatalysis for the $NtTiO_2$, $NtTiO_2$/NsCuO and Ti/TiO_2/CuO semiconductors.

At both electrodes, $NtTiO_2$/NsCuO and $NtTiO_2$, the photoelectrocatalytic conversion of CO_2 did not form measurable products, such as formic acid, acetic acid, formaldehyde, acetaldehyde, ethanol, propanol and acetone, analyzed in this work. In addition, the same reaction was performed by applying photocatalysis, without potential contribution, and it was not possible to quantify any of the products analyzed, even methanol. These results prove the contribution of the applied potential to the photocatalysis, as also observed by others authors [29,59–61].

The CO_2 reduction under potential of +0.2 V and UV–vis irradiation

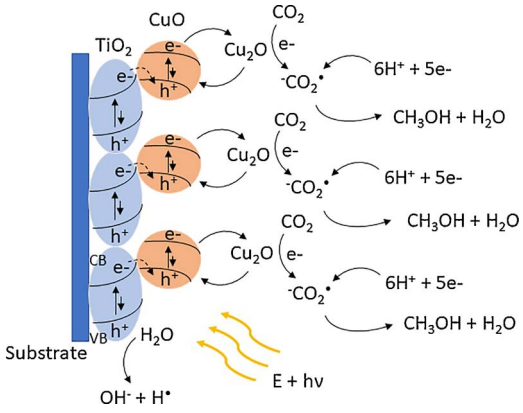

Fig. 7. Schematic representation of the charge-transfer mechanism in p-n junction $NtTiO_2$/NsCuO semiconductor under potential and UV–vis irradiation.

during 180 min of photoelectrocatalysis reached 0.1 mmol L^{-1} of methanol using $NtTiO_2$/NsCuO semiconductor, with 57% of faradaic efficiency (Fig. 6a, red curve). The methanol formation under nanotubes of TiO_2 without modification (Fig. 6a, black curve) reach less than 0.02 mmol L^{-1}, illustrating the importance of CuO nanospheres coating on CO_2 conversion. The process is based on the photogenerated electrons on the TiO_2 surface being trapped by the CuO, where the proper reduction reaction takes place [13].

The transfer mechanism of the $NtTiO_2$/NsCuO is initialized by the photons with energy higher than the band gap energy (E_g), which are absorved by the semiconductor (Fig. 7). The electrons with this energy are driven from the valence band (VB) to the conduction band (CB) of the TiO_2 nanotubes and CuO nanospheres, generating holes in the VB of both semiconductors. The electrons in the TiO_{2CB} are captured by holes generated in the CuO_{VB}, based on a Z-scheme mechanism. Thus, more electrons in the conduction band of CuO are free to react with electron acceptors (CO_2 in this case). The kinetic of reaction between holes and electrolyte (water) at $NtTiO_2$ is faster, generating hydrogen radical, as demonstrated in the Fig. 7. Thus, the efficiency of the CuO nanoparticle on the heterojunction composite is limited by (i) the kinetic of electron transfer in the interface, (ii) electron/hole recombination in the junction TiO_2 and CuO and (iii) the fast and efficient consumption of the hole presented in the n-type TiO_2 nanotubes [13,33,62], essential to form hydrocarbon.

Once EIS proved the presence of an improvement in the electrons transfers for $NtTiO_2$/NsCuO semiconductor, it suggests that, in a nanostructured p-n heterojunction electrode, the CO_2 conversion should be highly efficient due to a faster electron transfer. In addition, a more efficient hole is also operating, where hydrogen radicals are formed to generate methanol. Despite an improvement in the CO_2 reduction under $NtTiO_2$/NsCuO compared with $NtTiO_2$ without modification, the amount of methanol generated using the nanostructured $NtTiO_2$/NsCuO semiconductor and the Ti/TiO_2/CuO was the same, around

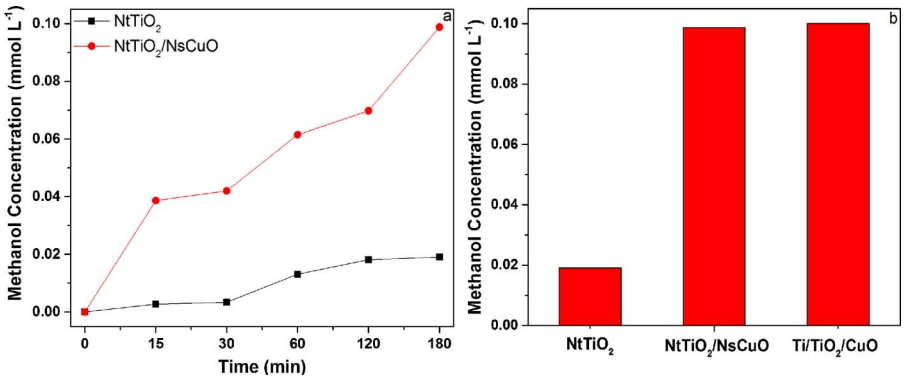

Fig. 6. a) Methanol formation during the time of photoelectrocatalysis under $NtTiO_2$ (black line) and $NtTiO_2$/NsCuO (red line) in 0.1 mol L^{-1} K_2SO_4 supporting electrolyte applying +0.20 V and UV–vis light; b) comparison of methanol concentration formed for the $NtTiO_2$, $NtTiO_2$/NsCuO and Ti/TiO_2/CuO semiconductors after 3 h of reaction. (For interpretation of the references to colour in this figure legend, the reader is referred to the web version of this article.)

0.1 mmol L^{-1} (Fig. 6b). There was no improvement in the catalytic process as it was expected. Hodes and coworkers [38] postulated that the efficiency exhibited by nanocrystals depends on the difference between electron and hole transfer into the supporting electrolyte. Therefore, there are two hypotheses for the low methanol production: (i) a large electron-hole pair recombination on the nanostructured semiconductor or (ii) a fast and efficient consumption of the hole presented in the n-type TiO_2 nanotubes by the product.

Once the photoelectrocatalysis proved to present a reduced charge recombination, promoting fast electron transfer to adsorbed CO_2, while at the same time maximizing the yield [[63],4,29,59], and the $NtTiO_2$ presents a very long photohole lifetime on the order of ms-s under conditions where water oxidation takes place [63], the hypothesis of the nanostructured heterojunction provide not just a more efficient electron transfer to CO_2, but also, a more efficient hole that is oxidizing the methanol generated seems more appropriated.

Taking in consideration that more efficient holes are operating in the $NtTiO_2$/NsCuO surface and that methanol is a known hole scavenger [64,65], reaching a hole trapping efficiency for TiO_2 semiconductor around 0.2 [65], the photoelectrocatalysis was carried out in the presence of glucose and p-nitrosodimethylaniline (RNO) as holes and OH scavenger, respectively [66–68]. Fig. 8a presents the photoelectrocatalytic reduction of CO_2 along the time using $NtTiO_2$/NpCuO carried out at in 0.1 mol L^{-1} K_2SO_4 under $E_{app} = +0.2$ V and UV–vis irradiation (curve I) and with addition of 0.05 mmol L^{-1} RNO (curve II) and 10.0 mmol L^{-1} glucose (curve III) in the supporting electrolyte.

The methanol formation increased six times when photoelectrocatalysis is carried out in the presence of hydroxyl radical scavenger (curve II). Therefore, according to these experiments, part of the methanol generated by the CO_2 reduction can be reoxidized to CO_2 and water if the product keeps in contact with OH species, due to the improvement in the charge transfer. The presence of OH species is confirmed in the Fig. 8b by the results of RNO discoloration (proportional to hydroxyl generation [66,67,69]) concomitantly to an experiment of CO_2 reduction on the heterojunction $NtTiO_2$/NsCuO. The results indicate that radicals are formed in the compartment of the working electrode, diagnosed by the promptly discoloration of the reagent (Fig. 8b, curve II) at a scan rate of -0.017 min^{-1}. The analysis of the electrolyte presented in the counter electrode compartment indicates that no hydroxyl radicals are formed in the counter compartment during the experiment (Fig. 8b, curve I).

The same reaction was performed at the same experimental conditions for the non-nanostructured electrode (Ti/TiO_2/CuO) in 0.1 mol L^{-1} K_2SO_4 with 0.05 mmol L^{-1} RNO solution pH 8. RNO discoloration was evaluated during 180 min of photoelectrolysis and also the simultanous methanol formation. The rate of RNO discoloration was -0.005 min^{-1}, which is more than 3 times slower than at $NtTiO_2$/NsCuO electrode. The discoloration is proportional to the hydroxyl radicals formed in the reaction, so it is possible to affirm that under the non-nanostructured electrode there is less formation of the hydroxyl radicals. No discoloration was observed in the counter electrode also using the non-nanostructured semiconductor.

The methanol formation was analyzed after the reaction under 0.1 mol L^{-1} K_2SO_4 with 0.05 mmol L^{-1} RNO solution pH 8, and it was observed no significative improvement in the product concentration generated, the value reaches the same amount obtained in the reaction without RNO, around 0.1 mmol L^{-1}. In addition, the reaction was not selective to methanol, also small amount of ethanol and acetone were observed, in the same way that it was obtained in our previous study [13]. The behavior could be indicative that lower amount of hydroxyl radical generation does not interfere in the CO_2 reduction using the non-nanostructured electrode. This reinforces the evidence that under a complete nanostructured electrode, there is an efficient electron and hole separation, with fast charge transfer, but also a fast and efficient competitive consumption of the products.

Thus, the results are indicative that in the heterojunction electrode nanostructured (p-n type junction) electrons and holes are spatially separated owning a long lifetime and driven to the surface in agreement with charge affinity. Electrons are trapped in the reduction of CO_2 adsorbed preferentially on CuO surface (p-type semiconductor), but also the holes are simultaneously formed in the TiO_2 semiconductor surface, which are able to oxidase not only water, but the methanol generated as well, decreasing the reaction efficiency.

The methanol generated in the solution could be oxidized not only indirectly by OH species, but also directly by the holes on the $NtTiO_2$ surface, once it is known as hole scavenger [64,65]. Higher methanol formation was obtained in the photoelectrocatalytic CO_2 reduction with glucose in solution (Fig. 8a, curve III) yielding 0.71 mmol L^{-1} after 3 h, indicating that glucose, acting as a trap for holes, prevents the OH formation and consequently the oxidation of the product by both, hole and/or hydroxyl species, generating an increase of 13% in the methanol production, comparing with the reaction with RNO. The H species can be provided by the glucose oxidation or/and even by the supporting electrolyte. Furthermore, the H species are able to react with the $CO_2^{\bullet-}$ species and generate methanol without any type of product oxidation. The reactions involved in this study are explained in the chemical Eq. (1)–(7).

$$Cu^{II}O + e^- \rightarrow Cu^{I}O + CO_2 \rightarrow Cu^{II}O + CO_2^{\bullet -} \quad (1)$$

$$h^+ + H_2O \rightarrow H^+ + OH^{\bullet} \quad (2)$$

$$CO_2^{\bullet -} + 6H^+ + 5e^- \rightarrow CH_3OH + H_2O \quad (3)$$

$$CH_3OH + OH^{\cdot}(or\ h^+) \rightarrow CO_2 + H_2O \quad (4)$$

$$(CH_3)_2N{-}Ph{-}NO + HO^{\bullet} \rightarrow (CH_3)_2N{-}Ph{-}N(OH)O^{\bullet} \quad (5)$$

$$C_6H_{12}O_6 + h^+ \rightarrow C_6H_{11}O_6^{\bullet} + H^+ \quad (6)$$

$$2OH^- \rightarrow O_2 + 2H^+ + 4e^- \quad (7)$$

The use of heterojunction $NtTiO_2$/NsCuO promotes a spatial charge carrier's separation and CuO has the capacity of trapping the electrons promoted to the conduction band of the TiO_2 nanotubes. The hole and electrons become specially separated, which provides to both a long

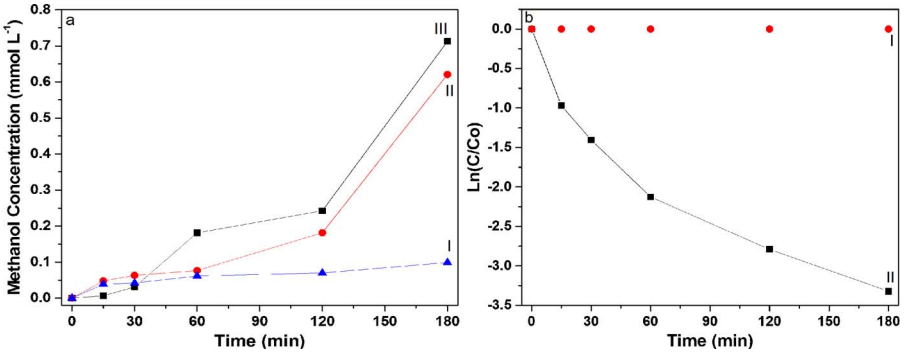

Fig. 8. a) CO_2 conversion into methanol at different times and applying photoelectrocatalysis at 0.2 V using 0.1 mol L^{-1} K_2SO_4 solution pH 8 (I), 0.1 mol L^{-1} K_2SO_4 and 0.05 mmol L^{-1} RNO solution pH 8 (II), and 0.1 mol L^{-1} K_2SO_4 and 10.0 mmol L^{-1} glucose solution pH 8 (III) as the supporting electrolyte; b) production rate of the steady state hydroxyl radical during photoelectrocatalytic CO_2 reduction at $NtTiO_2$/NsCuO electrode in 0.1 mol L^{-1} K_2SO_4 with 0.05 mmol L^{-1} RNO solution pH 8 in the counter compartment (I) and working electrode (II).

lifetime, and NsCuO begin to be a charged surface, where the CO_2 will adsorb amplifying the reduction to CO_2^- as intermediate [13]. This one electron reduction step is the thermodynamic limit to form the intermediate and further subsequent reductions [70].

4. Conclusions

In this work is demonstrated that nanostructured $NtTiO_2$/NsCuO electrodes were successfully constructed by anodization and dip-coating. The semiconductor with CuO nanoparticles dispersed on the TiO_2 nanotubes showed a typical heterojunction (p-n type) properties. It was verified by the amplification in the semiconductor response under UV–vis light, higher charge carrier's separations, lower charge transfer resistance, lower flat band potential and good photoactivity behavior. The nanostructured $NtTiO_2$/NsCuO electrode presented a good response for CO_2 reduction under UV–vis light and low potential such as +0.2 V. The same reaction was performed by adding RNO to the supporting electrolyte and the methanol formation was six times higher, leading to the conclusion that part of the product generated by the CO_2 reduction can be reoxidized to CO_2 and water if the product is still in contact with OH species. Maximum conversion was obtained in 0.1 mol L^{-1} K_2SO_4 pH 8 containing 10.0 mmol L^{-1} glucose, due to the fact that no OH species could be formed in the presence of glucose, and consequently, non-formed products were oxidized in this case, generating 0.71 mmol L^{-1} methanol with great selectivity in relation to ethanol, acetone, formaldehyde, acetaldehyde, formic acid or acetic acid. All the experiments presented in this paper were conducted with the same prepared semiconductor, showing a stability over of 27 h of reaction under potential and light incidence.

Acknowledgments

The authors would like to express their deepest gratitude and indebtedness to the Brazilian Research Assistance Agency – FAPESP (2013/25343-8 and 2008/10449-7) and INCT (465571/2014-0) for the financial support granted during the course of this research.

References

[1] P. Li, J. Xu, H. Jing, C. Wu, H. Peng, J. Lu, H. Yin, Wedged N-doped CuO with more negative conductive band and lower overpotential for high efficiency photoelectric converting CO_2 to methanol, Appl. Catal. B Environ. 156–157 (2014) 134–140, http://dx.doi.org/10.1016/j.apcatb.2014.03.011.

[2] S. Xia, Y. Meng, X. Zhou, J. Xue, G. Pan, Z. Ni, Ti/ZnO – Fe_2O_3 composite: synthesis, characterization and application as a highly efficient photoelectrocatalyst for methanol from CO_2 reduction, Appl. Catal. B Environ. 187 (2016) 122–133.

[3] J.F. Brito, A.A. Silva, A.J. Cavalheiro, M.V.B. Zanoni, Evaluation of the parameters affecting the photoelectrocatalytic reduction of CO_2 to CH_3OH at Cu/Cu_2O electrode, Int. J. Electrochem. Sci. 9 (2014) 5961–5973.

[4] Q. Shen, Z. Chen, X. Huang, M. Liu, G. Zhao, High-yield and selective photoelectrocatalytic reduction of CO_2 to formate by metallic copper decorated Co_3O_4 nanotube arrays, Environ. Sci. Technol. 49 (2015) 5828–5835, http://dx.doi.org/10.1021/acs.est.5b00066.

[5] G. Centi, S. Perathoner, Towards solar fuels from water and CO_2, ChemSusChem 3 (2010) 195–208, http://dx.doi.org/10.1002/cssc.200900289.

[6] C. Ampelli, C. Genovese, G. Centi, R. Passalacqua, S. Perathoner, Nanoscale engineering in the development of photoelectrocatalytic cells for producing solar fuels, Top. Catal. 59 (2016) 757–771, http://dx.doi.org/10.1007/s11244-016-0547-5.

[7] S. Perathoner, G. Centi, D. Su, Turning perspective in photoelectrocatalytic cells for solar fuels, ChemSusChem 9 (2016) 345–357, http://dx.doi.org/10.1002/cssc.201501059.

[8] J.A. Herron, J. Kim, A.A. Upadhye, G.W. Huber, C.T. Maravelias, A general framework for the assessment of solar fuel technologies, Energy Environ. Sci. 8 (2015) 126–157, http://dx.doi.org/10.1039/C4EE01958J.

[9] H.L. Tuller, Solar to fuels conversion technologies: a perspective, Mater. Renew. Sustain. Energy 6 (2017) 3, http://dx.doi.org/10.1007/s40243-017-0088-2.

[10] J.A. Keith, E.A. Carter, Theoretical insights into pyridinium-based photoelectrocatalytic reduction of CO_2, J. Am. Chem. Soc. 134 (2012) 7580–7583, http://dx.doi.org/10.1021/ja300128e.

[11] G.G. Bessegato, T.T. Guaraldo, J.F. de Brito, M.F. Brugnera, M.V.B. Zanoni, Achievements and trends in photoelectrocatalysis: from environmental to energy applications, Electrocatalysis 6 (2015) 415–441, http://dx.doi.org/10.1007/s12678-015-0259-9.

[12] J.F. Brito, A.R. Araujo, K. Rajeshwar, M.V.B. Zanoni, Photoelectrochemical reduction of CO_2 on Cu/Cu_2O films: product distribution and pH effects, Chem. Eng. J. 264 (2015) 302–309, http://dx.doi.org/10.1016/j.cej.2014.11.081.

[13] J.F. De Brito, M.V.B. Zanoni, On the application of Ti/TiO_2/CuO n-p junction semiconductor: a case study of electrolyte, temperature and potential influence on CO_2 reduction, Chem. Eng. J. 318 (2017) 264–271, http://dx.doi.org/10.1016/j.cej.2016.08.033.

[14] D. Guzmán, M. Isaacs, I. Osorio-Román, M. García, J. Astudillo, M. Ohlbaum, Photoelectrochemical reduction of carbon dioxide on quantum-dot-modified electrodes by electric field directed layer-by-layer assembly methodology, ACS Appl. Mater. Interfaces 7 (2015) 19865–19869, http://dx.doi.org/10.1021/acsami.5b05722.

[15] S. Stülp, J.C. Cardoso, J.F. de Brito, J.B.S. Flor, R.C.G. Frem, F.A. Sayão, M.V.B. Zanoni, An artificial photosynthesis system based on Ti/TiO_2 coated with Cu (II) aspirinate complex for CO_2 reduction to methanol, Electrocatalysis (2017) 1–9, http://dx.doi.org/10.1007/s12678-017-0367-9.

[16] K. Rajeshwar, N.R. De Tacconi, G. Ghadimkhani, W. Chanmanee, C. Janáky, Tailoring copper oxide semiconductor nanorod arrays for photoelectrochemical reduction of carbon dioxide to methanol, ChemPhysChem 14 (2013) 2251–2259, http://dx.doi.org/10.1002/cphc.201300080.

[17] S. Xie, Q. Zhang, G. Liu, Y. Wang, Photocatalytic and photoelectrocatalytic reduction of CO_2 using heterogeneous catalysts with controlled nanostructures, Chem. Commun. 52 (2015) 35–59, http://dx.doi.org/10.1039/C5CC07613G.

[18] G. Magesh, E.S. Kim, H.J. Kang, M. Banu, J.Y. Kim, J.H. Kim, J.S. Lee, A versatile photoanode-driven photoelectrochemical system for conversion of CO_2 to fuels with high faradaic efficiencies at low bias potentials, J. Mater. Chem. A 2 (2014) 2044, http://dx.doi.org/10.1039/c3ta14408a.

[19] G. Ghadimkhani, N.R. de Tacconi, W. Chanmanee, C. Janaky, K. Rajeshwar, Efficient solar photoelectrosynthesis of methanol from carbon dioxide using hybrid CuO-Cu_2O semiconductor nanorod arrays, Chem. Commun. (Camb.) 49 (2013) 1297–1299, http://dx.doi.org/10.1039/c2cc38068d.

[20] Y. Liu, H. Zhou, J. Li, H. Chen, D. Li, B. Zhou, W. Cai, Enhanced photoelectrochemical properties of Cu_2O-loaded short TiO_2 nanotube array electrode prepared by sonoelectrochemical deposition, Nano-Micro Lett. 2 (2010) 277–284, http://dx.doi.org/10.3786/nml.v2i.

[21] G. Yin, M. Nishikawa, Y. Nosaka, N. Srinivasan, D. Atarashi, E. Sakai, M. Miyauchi, Photocatalytic carbon dioxide reduction by copper oxide nanocluster-grafted niobate nanosheets, ACS Nano 9 (2015) 2111–2119, http://dx.doi.org/10.1021/nn507429e.

[22] K. Chiang, R. Amal, T. Tran, Photocatalytic degradation of cyanide using titanium dioxide modified with copper oxide, Adv. Environ. Res. 6 (2002) 471–485, http://dx.doi.org/10.1016/S1093-0191(01)00074-0.

[23] H.W. Slamet, E. Nasution, K. Purnama, J. Riyani, Gunlazuardi, Effect of copper species in a photocatalytic synthesis of methanol from carbon dioxide over copper-doped titania catalysts, World Appl. Sci. J. 6 (2009) 112–122.

[24] S. Qin, F. Xin, Y. Liu, X. Yin, W. Ma, Photocatalytic reduction of CO_2 in methanol to methyl formate over CuO-TiO_2 composite catalysts, J. Colloid Interface Sci. 356 (2011) 257–261, http://dx.doi.org/10.1016/j.jcis.2010.12.034.

[25] M.J. Siegfried, K.-S. Choi, Conditions and mechanism for the anodic deposition of cupric oxide films in slightly acidic aqueous media, J. Electrochem. Soc. 154 (2007) D674, http://dx.doi.org/10.1149/1.2789394.

[26] Z. Zhang, P. Wang, Highly stable copper oxide composite as an effective photocathode for water splitting via a facile electrochemical synthesis strategy, J. Mater. Chem. 22 (2012) 2456, http://dx.doi.org/10.1039/c1jm14478b.

[27] A. Paracchino, V. Laporte, K. Sivula, M. Grätzel, E. Thimsen, Highly active oxide photocathode for photoelectrochemical water reduction, Nat. Mater. 10 (2011) 456–461, http://dx.doi.org/10.1038/nmat3017.

[28] K. Bhattacharyya, A. Danon, B.K. Vijayan, K.A. Gray, P.C. Stair, E. Weitz, Role of the surface Lewis acid and base sites in the adsorption of \cf{CO_2} on titania nanotubes and platinized titania nanotubes: an in situ FT-IR study, J. Phys. Chem. C 117 (2013) 12661–12678, http://dx.doi.org/10.1021/jp402979m.

[29] T.T. Guaraldo, J.F. de Brito, D. Wood, M.V.B. Zanoni, A new Si/TiO_2/Pt p-n junction semiconductor to demonstrate photoelectrochemical CO_2 conversion, Electrochim. Acta 185 (2015) 117–124, http://dx.doi.org/10.1016/j.electacta.2015.10.077.

[30] M.R. Hasan, S.B. Abd Hamid, W.J. Basirun, S.H. Meriam Suhaimy, A.N. Che Mat, A sol–gel derived, copper-doped, titanium dioxide–reduced graphene oxide nanocomposite electrode for the photoelectrocatalytic reduction of CO_2 to methanol and formic acid, RSC Adv. 5 (2015) 77803–77813, http://dx.doi.org/10.1039/c5ra12525a.

[31] J. Liu, H. Shi, Q. Shen, C. Guo, G. Zhao, Efficiently photoelectrocatalyze CO_2 to methanol using Ru(II)-pyridyl complex covalently bonded on TiO_2 nanotube arrays, Appl. Catal. B Environ. 210 (2017) 368–378, http://dx.doi.org/10.1016/j.apcatb.2017.03.060.

[32] S. Sato, T. Arai, T. Morikawa, K. Uemura, T.M. Suzuki, H. Tanaka, T. Kajino, Selective CO_2 conversion to formate conjugated with H_2O oxidation utilizing semiconductor/complex hybrid photocatalysts, J. Am. Chem. Soc. 133 (2011) 15240–15243, http://dx.doi.org/10.1021/ja204881d.

[33] S.J.A. Moniz, J. Tang, Charge transfer and photocatalytic activity in CuO/TiO_2 nanoparticle heterojunctions synthesised through a rapid, one-pot, microwave solvothermal route, ChemCatChem 7 (2015) 1659–1667, http://dx.doi.org/10.1002/cctc.201500315.

[34] G.K. Mor, O.K. Varghese, R.H.T. Wilke, S. Sharma, K. Shankar, T.J. Latempa, K.S. Choi, C.A. Grimes, p-type Cu-Ti-O nanotube arrays and their use in self-biased heterojunction photoelectrochemical diodes for hydrogen generation, Nano Lett. 8 (2008) 1906–1911, http://dx.doi.org/10.1021/nl080572y.

[35] Y. Xu, Y. Jia, Y. Zhang, R. Nie, Z. Zhu, J. Wang, H. Jing, Photoelectrocatalytic reduction of CO_2 to methanol over the multi-functionalized TiO_2 photocathodes, Appl. Catal. B Environ. 205 (2017) 254–261, http://dx.doi.org/10.1016/j.apcatb.2016.12.039.
[36] I. Paramasivam, H. Jha, N. Liu, P. Schmuki, A review of photocatalysis using self-organized TiO_2 nanotubes and other ordered oxide nanostructures, Small 8 (2012) 3073–3103, http://dx.doi.org/10.1002/smll.201200564.
[37] C. Adán, J. Marugán, E. Sánchez, C. Pablos, R. Van Grieken, Understanding the effect of morphology on the photocatalytic activity of TiO_2 nanotube array electrodes, Electrochim. Acta 191 (2016) 521–529, http://dx.doi.org/10.1016/j.electacta.2016.01.088.
[38] G. Hodes, I.D.J. Howell, L.M. Peter, A new concept in photovoltaic cells, J. Electrochem. Soc. 139 (1992) 3136.
[39] D. Jiang, H. Zhao, S. Zhang, R. John, Kinetic study of photocatalytic oxidation of adsorbed carboxylic acids at TiO_2 porous films by photoelectrolysis, J. Catal. 223 (2004) 212–220, http://dx.doi.org/10.1016/j.jcat.2004.01.030.
[40] G.G. Bessegato, J.C. Cardoso, B.F. Da Silva, M.V.B. Zanoni, Enhanced photoabsorption properties of composites of Ti/TiO_2 nanotubes decorated by Sb_2S_3 and improvement of degradation of hair dye, J. Photochem. Photobiol. A Chem. 276 (2014) 96–103, http://dx.doi.org/10.1016/j.jphotochem.2013.12.001.
[41] L. Perazolli, L. Nuñez, M.R.A. da Silva, G.F. Pegler, A.G.C. Costalonga, R. Gimenes, M.M. Kondo, M.A.Z. Bertochi, TiO_2/CuO films obtained by citrate precursor method for photocatalytic application, Mater. Sci. Appl. 2 (2011) 564–571, http://dx.doi.org/10.4236/msa.2011.26075.
[42] R.M. Fabrao, J.F. de Brito, J.L. da Silva, N.R. Stradiotto, M.V.B. Zanoni, Appraisal of photoelectrocatalytic oxidation of glucose and production of high value chemicals on nanotube Ti/TiO_2 electrode, Electrochim. Acta. 222 (2016) 123–132, http://dx.doi.org/10.1016/j.electacta.2016.10.164.
[43] G.G. Bessegato, J.C. Cardoso, M.V.B. Zanoni, Enhanced photoelectrocatalytic degradation of an acid dye with boron-doped TiO_2 nanotube anodes, Catal. Today 240 (2015) 100—106, http://dx.doi.org/10.1016/j.cattod.2014.03.073.
[44] J. Tauc, R. Grigorovici, A. Vancu, Optical properties and electronic structure of amorphous germanium, Phys. Status Solidi 15 (1966) 627–637.
[45] M. Izaki, M. Nagai, K. Maeda, F.B. Mohamad, K. Motomura, J. Sasano, T. Shinagawa, S. Watase, Electrodeposition of 1.4-eV-bandgap p-copper (II) oxide film with excellent photoactivity, J. Electrochem. Soc. 158 (2011) D578, http://dx.doi.org/10.1149/1.3614408.
[46] Y.F. Lim, J.J. Choi, T. Hanrath, Facile synthesis of colloidal CuO nanocrystals for light-harvesting applications, J. Nanomater. 2012 (2012), http://dx.doi.org/10.1155/2012/393160.
[47] T.T. Guaraldo, T.B. Zanoni, S.I.C. de Torresi, V.R. Gonçales, G.J. Zocolo, D.P. Oliveira, M.V.B. Zanoni, On the application of nanostructured electrodes prepared by Ti/TiO_2/WO_3 "template": a case study of removing toxicity of indigo using visible irradiation, Chemosphere 91 (2013) 586–593, http://dx.doi.org/10.1016/j.chemosphere.2012.12.027.
[48] L. Jing, B. Xin, F. Yuan, L. Xue, B. Wang, H. Fu, Effects of surface oxygen vacancies on photophysical and photochemical processes of Zn-doped TiO_2 nanoparticles and their relationships, J. Phys. Chem. B 110 (2006) 17860–17865, http://dx.doi.org/10.1021/jp063148z.
[49] Y. Cai, Y. Ye, Z. Tian, J. Liu, Y. Liu, C. Liang, In situ growth of lamellar $ZnTiO_3$ nanosheets on TiO_2 tubular array with enhanced photocatalytic activity, Phys. Chem. Chem. Phys. 15 (2013) 20203–20209, http://dx.doi.org/10.1039/c3cp53307g.
[50] G.R. Torres, T. Lindgren, J. Lu, C.G. Granqvist, S.E. Lindquist, Photoelectrochemical study of nitrogen-doped titanium dioxide for water oxidation, J. Phys. Chem. B. 108 (2004) 5995–6003, http://dx.doi.org/10.1021/Jp037477s.
[51] B. Neumann, P. Bogdanoff, H. Tributsch, S. Sakthivel, H. Kisch, Electrochemical mass spectroscopic and surface photovoltage studies of catalytic water photooxidation by undoped and carbon-doped titania, J. Phys. Chem. B 109 (2005) 16579–16586, http://dx.doi.org/10.1021/jp051339g.
[52] T. Lindgren, J.M. Mwabora, E. Avendaño, J. Jonsson, A. Hoel, C.-G. Granqvist, S.-E. Lindquist, Photoelectrochemical and optical properties of nitrogen doped titanium dioxide films prepared by reactive DC magnetron sputtering, J. Phys. Chem. B 107 (2003) 5709–5716, http://dx.doi.org/10.1021/jp027345j.
[53] S. Chai, G. Zhao, Y.N. Zhang, Y. Wang, F. Nong, M. Li, D. Li, Selective photoelectrocatalytic degradation of recalcitrant contaminant driven by an n-P heterojunction nanoelectrode with molecular recognition ability, Environ. Sci. Technol. 46 (2012) 10182–10190, http://dx.doi.org/10.1021/es3021342.
[54] X. Cheng, H. Liu, Q. Chen, J. Li, P. Wang, Preparation and characterization of palladium nano-crystallite decorated TiO_2 nano-tubes photoelectrode and its enhanced photocatalytic efficiency for degradation of diclofenac, J. Hazard. Mater. 254–255 (2013) 141–148, http://dx.doi.org/10.1016/j.jhazmat.2013.03.062.
[55] A.G. Muñoz, Q. Chen, P. Schmuki, Interfacial properties of self-organized TiO_2 nanotubes studied by impedance spectroscopy, J. Solid State Electrochem. 11 (2007) 1077–1084, http://dx.doi.org/10.1007/s10008-006-0241-9.
[56] G.G. Bessegato, F.F. Hudari, M.V.B. Zanoni, Self-doped TiO_2 nanotube electrodes: a powerful tool as a sensor platform for electroanalytical applications, Electrochim. Acta. 235 (2017) 527–533, http://dx.doi.org/10.1016/j.electacta.2017.03.141.
[57] P.E. de Jongh, D. Vanmaekelbergh, J.J. Kelly, Photoelectrochemistry of electrodeposited Cu_2O, J. Electrochem. Soc. 147 (2000) 486, http://dx.doi.org/10.1149/1.1393221.
[58] T.J. Richardson, J.L. Slack, M.D. Rubin, Electrochromism in copper oxide thin films, Electrochim. Acta 46 (2001) 2281–2284, http://dx.doi.org/10.1016/S0013-4686(01)00397-8.
[59] H. Peng, J. Lu, C. Wu, Z. Yang, H. Chen, W. Song, P. Li, H. Yin, Co-doped MoS_2 NPs with matched energy band and low overpotential high efficiently convert CO_2 to methanol, Appl. Surf. Sci. 353 (2015) 1003–1012, http://dx.doi.org/10.1016/j.apsusc.2015.06.178.
[60] P. Li, J. Zhang, H. Wang, H. Jing, J. Xu, X. Sui, H. Hu, H. Yin, The photoelectric catalytic reduction of CO_2 to methanol on CdSeTe NSs/TiO_2 NTs, Catal. Sci. Technol. 4 (2014) 1070, http://dx.doi.org/10.1039/c3cy00978e.
[61] J. Cheng, M. Zhang, J. Liu, J. Zhou, K. Cen, A Cu foam cathode used as a Pt – RGO catalyst matrix to improve CO_2 reduction in a photoelectrocatalytic cell with a TiO_2 photoanode, J. Mater. Chem. A Mater. Energy Sustain. 3 (2015) 12947–12957, http://dx.doi.org/10.1039/C5TA03026A.
[62] C.G. Morales-Guio, S.D. Tilley, H. Vrubel, M. Grätzel, X. Hu, Hydrogen evolution from a copper(I) oxide photocathode coated with an amorphous molybdenum sulphide catalyst, Nat. Commun. 5 (2014) 3059, http://dx.doi.org/10.1038/ncomms4059.
[63] A.J. Cowan, J.R. Durrant, Long-lived charge separated states in nanostructured semiconductor photoelectrodes for the production of solar fuels, Chem. Soc. Rev. 42 (2013) 2281–2293, http://dx.doi.org/10.1039/c2cs35305a.
[64] X. Zhang, H. Cui, M. Humayun, Y. Qu, N. Fan, X. Sun, L. Jing, Exceptional performance of photoelectrochemical water oxidation of single-crystal rutile TiO_2 nanorods dependent on the hole trapping of modified chloride, Sci. Rep. 6 (2016) 21430, http://dx.doi.org/10.1038/srep21430.
[65] T.L. Thompson, J.T. Yates Jr, Monitoring hole trapping in photoexcited TiO_2(110) using a surface photoreaction, J. Phys. Chem. B. 109 (2005) 18230–18236, http://dx.doi.org/10.1021/jp0530451.
[66] C. Kim, S. Kim, J. Choi, J. Lee, J.S. Kang, Y.E. Sung, J. Lee, W. Choi, J. Yoon, Blue TiO_2 nanotube array as an oxidant generating novel anode material fabricated by simple cathodic polarization, Electrochim. Acta 141 (2014) 113–119, http://dx.doi.org/10.1016/j.electacta.2014.07.062.
[67] J. Muff, L.R. Bennedsen, E.G. Søgaard, Study of electrochemical bleaching of p-nitrosodimethylaniline and its role as hydroxyl radical probe compound, J. Appl. Electrochem. 41 (2011) 599–607, http://dx.doi.org/10.1007/s10800-011-0268-1.
[68] G. Kim, S.H. Lee, W. Choi, Glucose-TiO_2 charge transfer complex-mediated photocatalysis under visible light, Appl. Catal. B Environ. 162 (2015) 463–469, http://dx.doi.org/10.1016/j.apcatb.2014.07.027.
[69] M.E. Simonsen, J. Muff, L.R. Bennedsen, K.P. Kowalski, E.G. Sogaard, Photocatalytic bleaching of p-nitrosodimethylaniline and a comparison to the performance of other AOP technologies, J. Photochem. Photobiol. A Chem. 216 (2010) 244–249, http://dx.doi.org/10.1016/j.jphotochem.2010.07.008.
[70] G.K. Ramesha, J.F. Brennecke, P.V. Kamat, The origin of catalytic effect in the reduction of CO_2 at nanostructured TiO_2 films, ACS Catal. 4 (2014) 3249–3254, http://dx.doi.org/10.1021/cs500730w.